Eur. Phys. J. D **26**, 99–104 (2003)
DOI: 10.1140/epjd/e2003-00201-y

THE EUROPEAN PHYSICAL JOURNAL D

Atomic and molecular ions in intense ultra-fast laser fields

W.R. Newell[1], I.D. Williams[2], and W.A. Bryan[1,a]

[1] Department of Physics and Astronomy, University College London, Gower Street, London WC1E 6BT, UK
[2] Department of Physics, Queen's University Belfast, Belfast BT7 1NN, UK

Received 6 January 2003
Published online 15 July 2003

Abstract. The interaction of a 60 fs 790 nm laser pulse with beams of Ar^+, C^+, H_2^+, HD^+ and D_2^+ are discussed. Intensities up to 10^{16} Wcm^{-2} are employed. An experimental z-scanning technique is used to resolve the intensity dependent processes in the confocal volume.

PACS. 32.80.Fb Photoionization of atoms and ions – 33.80.Rv Multiphoton ionization and excitation to highly excited states (e.g., Rydberg states) – 42.50.Hz Strong-field excitation of optical transitions in quantum systems; multiphoton processes; dynamic Stark shift

1 Introduction

Recent advances in laser technology have lead to the routine availability of high intensity (>10^{13} Wcm^{-2}), ultra-fast (<100 fs) laser pulses [1], which may be focussed to generate electric fields capable of severing the electron-proton bond in the hydrogen atom. Such conditions have opened up a new field of research into intense laser — matter interactions. In the atomic case, following initial ionization [2], the behaviour of the departing electron has been found to be influential in the ionization of noble gas targets [3,4]. Experimental observations of intensity dependent ion yields have identified the importance of the interplay between sequential and non-sequential ionization [3–5]. S-matrix theory [6] and evaluation of the time-dependent Schrödinger equation [7] have provided quantitative agreements with experiment, and quasiclassical tunnelling (ADK) theory [8] has been also partially successful.

When molecules are exposed to similar laser conditions, a number of additional complex phenomena have been observed. Above-threshold dissociation (ATD), bond-softening [9] and bond-hardening [10] have been observed in H_2, universally discussed in terms of light-induced potentials, for a discussion see [11]. In a broad range of polyatomic molecules, a kinetic energy defect has been observed [12], explained variously by a classical enhancement of the ionization probability through electron localization [13], charge resonance caused by a coupling of the Stark shift to the electron population [14] and a hydrodynamic Thomas-Fermi treatment of the system [15].

[a] e-mail: w.bryan@ucl.ac.uk

2 Experimental

In the present laser-ion studies, the intense field phenomena were initiated by allowing the CPA [16] output of a Ti:sapphire laser system to interact with a beam of target ions. The RAL (UK) ASTRA laser system generated pulses with an approximately Gaussian temporal profile of 60 fs FWHM at a wavelength of 790 nm at a 10 Hz repetition rate. The laser beam was focussed by a $f/25$ lens producing a Gaussian beam waist of 16 μm. The laser focus could be translated parallel to the beam propagation direction (z-axis), allowing the ion beam to interact with different regions of the focal volume, a technique referred to as z-scanning. A plasma discharge ion source was used to generate the target ion beam [17,18]. Typically, the ions were extracted with a kinetic energy of 1 keV, momentum selected by a bending magnet and focussed into the interaction region to a diameter of 1.5 mm FWHM. The ion beam currents at this point were typically 50 nA and 1 μA for atomic and molecular ions respectively. The ion beam apparatus is illustrated schematically in Figure 1. Further details of the experimental apparatus are given in [17,18].

After passing through the laser focus, the reaction products entered a 45° parallel plate analyser. The primary beam was steered into a well-baffled Faraday cup, separating it from the ionic fragments. These were detected in an off-axis channel electron multiplier (CEM). The kinetic energy of these particles was measured by applying a variable electric field to a pair of deflection plates at the entrance to the parallel plate analyser. Neutral reaction products passed undeflected into a second on-axis CEM. Time-of-flight (ToF) analysis was used to calculate the kinetic energy of these products.

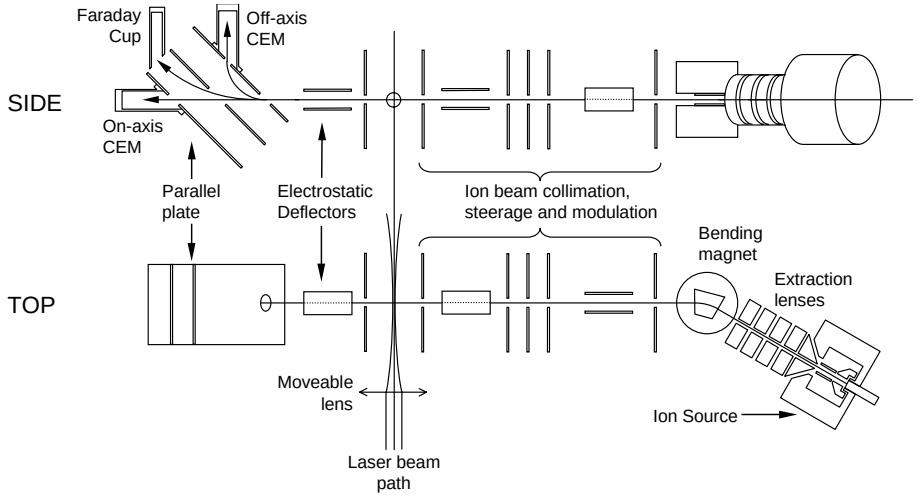

Fig. 1. Schematic of the crossed-beam apparatus.

3 Atomic ions

The proposed "atomic antenna" [19] or "recollision" [20,21] model has been used to describe observations of non-sequential ionization in neutral atoms [3–5]. Starting with a neutral atomic target, primary ionization is either *via* multiphoton ionization (MPI) or tunnelling through the atomic potential distorted by the external field. The departing electron is accelerated by the external field and, depending on the initial phase can return to the singly charged ion with energies up to $3.17U_P$ [4], where U_P is the classical pondermotive energy in the field. Further ionization can proceed by ionizing collisions, tunnelling from the ionized species or ionic excitation combined with tunnelling. In the crossed ion beam-laser system, primary ionization is accomplished prior to the arrival of the laser pulse, allowing, for the first time, decoupling of the sequential and non-sequential processes for the first stage of ionization. In the atomic cases discussed in the following sections, Ar^+ and C^+ ions form the laser target. It is well-known that atomic ions produced in a plasma discharge source are a mixture of the ground and metastable states [22]. However, using the z-scan technique the ion beam components have been resolved, and a number of new observations made. Figure 2 shows a simplified energy level diagram for (a) an Ar^+ beam and (b) a C^+ beam, where possible ionizing transitions are indicated by arrows.

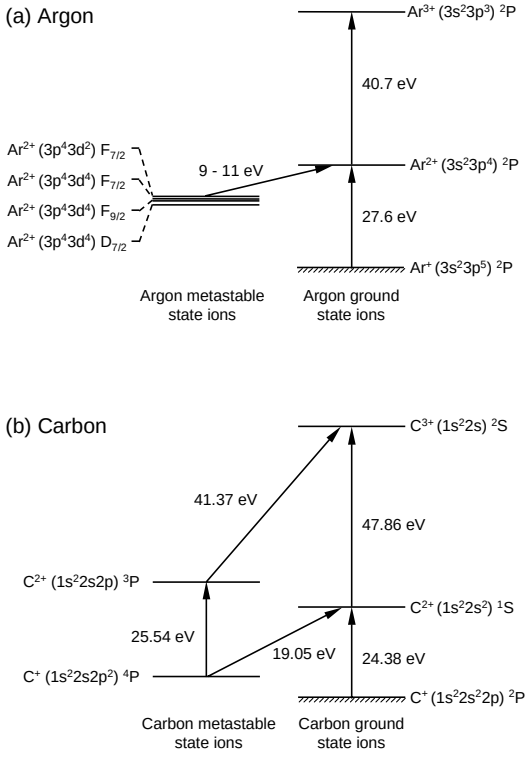

Fig. 2. Energy level diagrams depicting the ionizing transitions observed in Ar^+ and C^+ ion beams irradiated with 60 fs laser pulses.

3.1 Ionization of Ar^+

Figure 3 shows the measured Ar^{2+} z-scan signal profile at peak intensities of 10^{16} and 5×10^{15} Wcm^{-2}, resulting from field-ionization of the primary Ar^+ beam. Each point represents the integral under the Ar^{2+} peak in the corresponding time-of-flight spectrum. The sharp peak observed at $z = 0$, *i.e.* the maximum focused intensity, is due to single ionization of ground state $(3s^2 3p^5)$ ^2P Ar^+ ions. The two peaks on either side of the zero position are due to the ionization of a small fraction of metastable Ar^+ ions, lying between 16 and 19 eV above the ground state [23]. These long-lived states are $(3p^4 3d^4)$ $D_{7/2}$ (16.4 eV), $(3p^4 3d^4)$ $F_{9/2}$ (17.6 eV), $(3p^4 3d^4)$ $F_{7/2}$ (17.7 eV) and $(3p^4 3d^2)$ $F_{7/2}$ (18.5 eV). This process is illustrated in Figure 2a. The signal profile results from the interplay of increasing interaction volume with decreasing intensity as the lens moves away from zero. The ionization potentials for the metastable components are

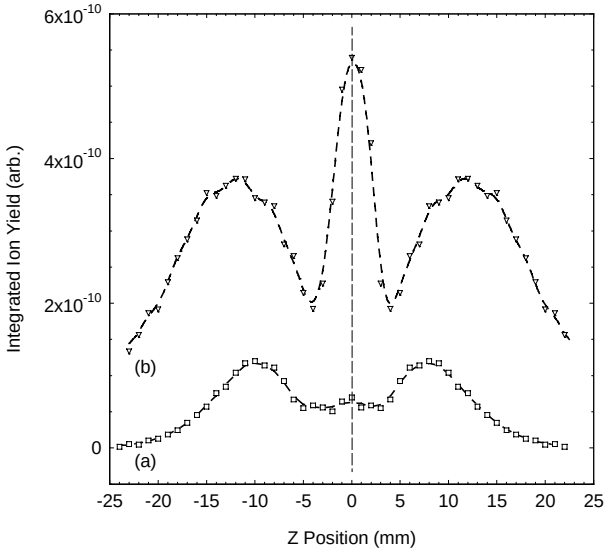

Fig. 3. Ar^{2+} production from an Ar^{+} ion beam as a function of focusing lens position (z), where $z = 0$ mm corresponds to the maximum intensity in the focus overlapping with the ion beam. Two peak intensities were used: (a) 5×10^{15} Wcm^{-2} and (b) 10^{16} Wcm^{-2}.

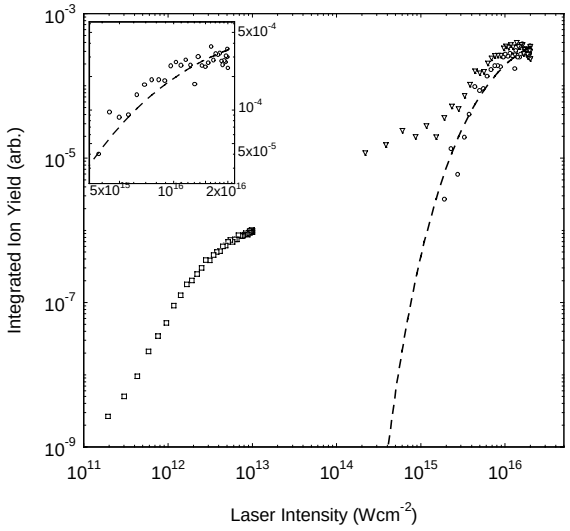

Fig. 4. Ar^{2+} production from a beam of Ar^{+} as a function of local peak intensity. Low intensity data (squares) were taken at $z = 12$ mm, high intensity at $z = 0$ mm. The circles show the metastable subtracted component representing Ar^{2+} from ground state Ar^{+}, and the dashed curve shows the ADK fit. An expanded view is shown in the insert.

approximately 9–11 eV, compared with 27.6 eV for the ground state. It is clear that the ground state peak at $z = 0$ disappears rapidly compared to the peaks at $z = \pm 12$ mm as the intensity decreases.

The Ar^{2+} yield from Ar^{+} is shown as a function of local on axis peak intensity in Figure 4. The Ar^{2+} yield is comprised of two curves with the low intensity curve ($10^{11} \rightarrow 10^{13}$ Wcm^{-2}) obtained with the lens positioned at $z = 12$ and the high intensity ($10^{14} \rightarrow 10^{16}$ Wcm^{-2}) at $z = 0$. The lower intensity Ar^{2+} curve arises purely from the ensemble of metastable states whereas the higher intensity Ar^{2+} curve arises from ionization of both ground state and metastable Ar^{+}. The small component of the higher intensity Ar^{2+} curve lying between 10^{14} and 10^{15} Wcm^{-2} has a slope of 0.5 which is characteristic of the onset of saturated ionization from the Ar^{+} metastables in the diffraction rings surrounding the Airy disk [24].

To test the applicability of quasi-classical tunnelling (ADK) theory [8] to the Ar^{2+} results, we have calculated the ionization rate of ground state Ar^{+} to Ar^{2+}, shown in Figure 4 as the dashed curve. These calculations were performed after subtracting an estimate of the metastable contribution and allow for the variation in interaction volume with local peak intensity. As can be seen from the insert in Figure 4, the ADK theory fits the data well in the region $10^{15} \rightarrow 10^{16}$ Wcm^{-2} where the Keldysh parameter γ [25] is $0.5 \rightarrow 0.16$ in the range consistent with tunnelling ($\gamma < 1$). Multiple ionization of rare gas atoms has been studied theoretically [6] using intense field many-body S-matrix theory; in particular, intensity dependent triple-ionization yields for Ar^{3+} production from Ar generated by 200 fs laser pulses. While the different pulse lengths forbid a fully quantitative analysis, it is still instructive to make a comparison.

As discussed in detail in [26], the ion beam apparatus was used to measure the ratio of Ar^{3+} to Ar^{2+} production from Ar^{+} and a time-of-flight apparatus was used to measure the same ratio from an Ar target. After correction for the different interaction volumes in each case, the following ratios were found: Ar^{3+}:Ar^{2+}(Ar^{+} target) $= 0.007 \pm 0.002$ and Ar^{3+}:Ar^{2+}(Ar target) $= 0.038 \pm 0.002$. The ratios presented in [6] are Ar^{3+}:Ar^{2+}(Ar^{+} target) $= 0.03$ and Ar^{3+}:Ar^{2+}(Ar target) $= 0.04$. Hence, there is a strong agreement between [6] and our results from a neutral target, but not in the case of the Ar^{+} ion. However, at a corresponding intensity, an ADK prediction for purely sequential ionization gives a ratio of 0.01, much closer to the present value of 0.007.

These results show that the removal of an electron prior to the interaction with the laser pulse almost completely suppresses the nonsequential process, leaving a small contribution from sequential ionization.

3.2 Ionization of C^{+}

The ion source has recently been used to generate a beam of C^{+} ions from carbon monoxide. The laser focus was scanned through the ion beam generating C^{2+} ions, and the signal profile shown in Figure 5 measured, where the peak laser intensity of 3×10^{16} Wcm^{-2} is generated at $z = 0$. There are two features present in Figure 5: a peak at $z = 2.5$ mm, and a distinct shoulder at $z = 4.5$ mm. To identify the processes occurring in the laser focus, the intensity profile within the confocal volume was modelled, and the threshold intensities at these two positions calculated as 1.5×10^{15} and 3.6×10^{14} Wcm^{-2} for the main feature ($z = 2.5$ mm) and shoulder ($z = 4.5$ mm) respectively. These thresholds were used in a classical

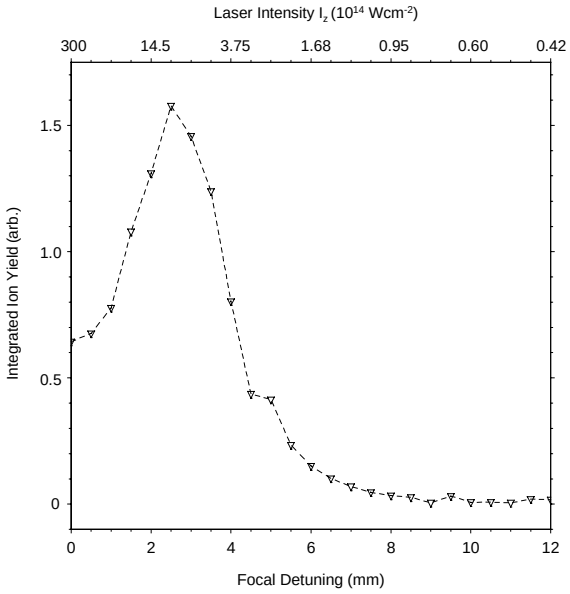

Fig. 5. C^{2+} production from a C^+ beam as a function of focussing lens position, recorded at a peak intensity of 3×10^{16} Wcm^{-2}.

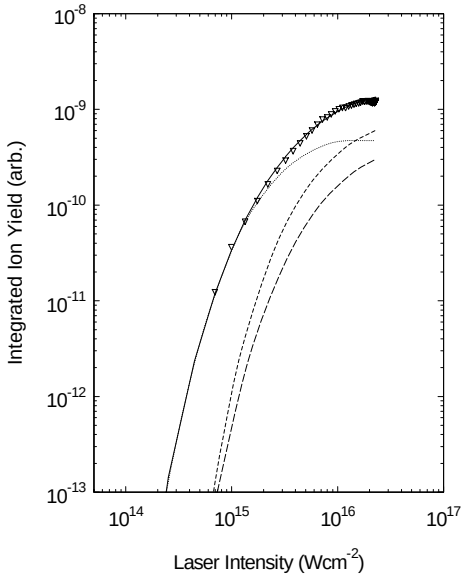

Fig. 6. C^{2+} production from a C^+ ion beam as a function of local on-axis peak intensities. Three ADK curves are summed to generate the fit to the experimental data (solid line). The three processes are: 19.05 eV (short dashed line), 24.38 eV (dotted line) and 25.54 eV (long dashed line).

over-the-barrier ionization model to identify the ionization potentials of the two processes, which are 24 eV ($z = 2.5$ mm) and 19 eV ($z = 4.5$ mm).

Returning to Figure 2b, the C^+ ionization processes are identified thus. There is an unresolved overlap in energy between the observed processes occurring at approximately 24 eV. The transitions from the C^+ $(1s^2 2s^2 2p)$ $^2P^0$ ground state to the C^{2+} $(1s^2 2s^2)$ ^1S ground state of C^{2+} occurs at 24.36 eV, and that from the C^+ $(1s^2 2s 2p^2)$ ^4P metastable to the C^{2+} ground state occurs at 19.05 eV. Given that we have already observed metastable argon ions [26] from the plasma discharge source, it is reasonable that a small fraction of C^+ metastables are present. With this in mind, the 25.54 eV transition from the C^+ $(1s^2 2s 2p^2)$ ^4P metastable to the C^{2+} $(1s^2 2s 2p)$ ^3P metastable is also energetically favourable but unresolved from the process at 24.36 eV.

Out of the possible terms (^2S, ^2P, ^2D and ^4P) arising from the $(1s^2 2s 2p^2)$ configuration, only the ^4P ($J = 1/2$, 3/2, 5/2) C^+ metastable state (all three spins aligned) will be present at the interaction region. This is because the other terms are optically coupled to the $(1s^2 2s^2 2p)$ ^2P C^+ ground state, and will decay during transport of the ion beam to the interaction region (typically 1 μs). Therefore, unlike the other ionizing transitions, removal of a p-shell electron from the C^+ $(1s^2 2s^2 2p^2)$ ^4P quartet will leave the atomic core with both spins aligned, rather than the desired spin-up — spin-down singlet configuration of the C^{2+} ground state. In effect, the observed 19.05 eV ionizing transition at $z = 4.5$ mm appears to be spin forbidden. In order for the 19.05 eV pathway to proceed, the carbon ion quartet configuration must undergo a spin-flip such that the atomic residue, following ionization, occupies the ground state singlet configuration. In an intense laser field, spin-flipping transitions can proceed by a number of mechanisms, namely magnetic interaction, shake-down or Stark shifting. Although clearly present on the C^{2+} z-scan, the ion yield from this 19.05 eV C^+ metastable to C^{2+} ground state process is actually relatively small, and is only experimentally discernible due to the low intensity volume enhancement of the z-scan technique.

The ion yield as a function of peak laser intensity is shown in Figure 6. The sequential ionization mechanisms within these full-volume intensity dependent ion yields are well described by the ADK model as the process is saturated. However, unlike the free-parameter fit for Ar^+, the ADK fit to C^{2+} will be constrained, as the ionization potentials of the observed process define the effective principle quantum numbers as 1.69 and 1.51 for the 19 and 24 eV features respectively.

The C^{2+} signal as a function of laser intensity is described by a convolution of three ADK curves, namely a low intensity curve corresponding to metastable C^+ ionization into the C^{2+} ground state (19.05 eV), and higher intensity curves for the C^+ ground state to the C^{2+} ground state (24.38 eV) and the metastable C^+ to excited ^3P C^{2+} process (25.54 eV). By scaling these ADK curves against the experimental data, a best fit has been obtained yielding scaling factors for each curve. The scaling parameters for the three processes are: 0.17, 0.67 and 0.16 for the 19.05, 24.38 and 25.54 eV processes respectively.

By taking the ratio of just the 19.05 eV process to the 24.38 eV process (0.17:0.67) the ADK fit to the C^{2+} intensity scan data predicts a 1:4 metastable to ground state population for the initial C^+ ion beam. Importantly, this metastable population fraction is fully compatible with a completely independent C^+ ion metastable population

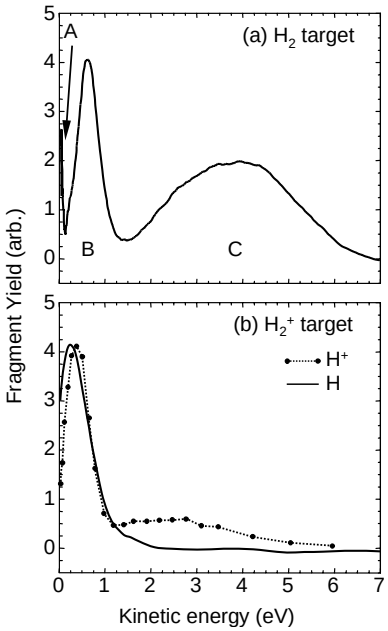

Fig. 7. Kinetic energy spectra from the interaction of the laser with (a) neutral H_2 gas target and (b) an H_2^+ ion beam, the solid line representing H from H_2^+, the filled circles representing H^+ from H_2^+.

measurement of 0.15 ± 0.07, determined through superelastic electron scattering using a similar ion source [27]. It is to be noted that the Keldysh parameter γ [25] for the data set in Figure 6 lies in the range 0.6 to 0.16, well within the tunnelling region.

4 Molecular ions

The fragmentation processes associated with the laser-H_2 interaction are ionization, dissociation $(0,1)$ and Coulomb explosion $(1,1)$. In the case of H_2^+, this fragmentation process is simplified to dissociation and Coulomb explosion; the channel notation (p,q) denotes the ionization multiplicity of the fragmenting particles. In general, the analysis of H_2 $(0,1)$ and H_2 $(1,1)$ processes is evaluated using the dynamics of H_2^+ $(0,1)$ and H_2^+ $(1,1)$ without little regard for the correlation of the primary ionized electron [11].

The three well-known observed peaks in the kinetic energy spectrum from the laser-H_2 interaction, as shown in Figure 7a, have been interpreted as being due to the bond-softening (A), above-threshold dissociation (B) and Coulomb explosion (C). In all cases, the laser wavelength is 790 nm and pulse length 60 fs.

The bond-softening mechanism may be understood in terms of light-dressed potentials and an adiabatic avoided curve crossing between the two lowest electronic states of the H_2^+ molecular ion ($1s\sigma_g$ and $2p\sigma_u$), coupled with a single photon absorption resonance. Ions in the vibrational level $v = 5$ of the $1s\sigma_g$ state can escape through the gap with close to zero dissociation energy, while those in higher vibrational levels will escape with correspondingly higher energies. A similar avoided crossing at the three photon absorption resonance (with one photon re-emitted, leading to a net two photon process) has been invoked to explain the above threshold dissociation peak, occurring from the $v = 3$ vibrational level. The Coulomb explosion peak results from enhanced ionization [13–15] subsequent to dissociation at some critical internuclear separation r_c of the H_2^+ ion, where $r_c > r_e$, where r_e is the equilibrium internuclear separation of the molecular ion.

Significantly different is the proton spectrum obtained using H_2^+ as the target, as shown in Figure 7b, in which only two peaks are observed. The Coulomb explosion peak is clearly identified to be in the same region as that observed using H_2 while only a single low energy peak at 0.2 eV is observed. Although this peak is quite broad in energy, the position of the peak suggests that the one photon process is dominant in the present measurements, with the possibility of some contribution from the two photon process. This in the exact reverse of the observation in H_2 at similar intensities. Also shown in Figure 7b is the spectrum obtained by observing the H neutral from the $(0,1)$ dissociation of H_2^+. Since in this case there is no $(1,1)$ channel, the neutral spectrum in Figure 7b provides an opportunity to observe the three photon peak, predicted to occur at a fragment energy of 1.3 eV. This is due to the absorption of three photons, but avoiding the re-emission of one photon. In high pulse intensity experiments such a peak would always be hidden below the Coulomb explosion peak in a proton spectrum, but if present would be evident in a neutral spectrum. In the present study there does appear to be a distinct shoulder on the high energy tail of the $(0,1)$ H atom spectrum at 1.3 eV which is indicative of a three photon process. A full analysis of the three photon process is given by [28] in this volume, and more complete discussions of the fragmentation dynamics and vibrational population distributions are given in [18,29].

In addition, by rotating the laser polarization by ϕ, where $\phi = 0$ locates the polarization axis parallel to the incident ion beam, the intensity of the product H and D atoms from H_2^+, HD^+ and D_2^+ are obtained. In all cases, a $\cos^2\phi$ distribution is observed, as shown in Figure 8. This is in marked contrast to the $\cos^n\phi$ distribution $(n = 8)$ observed for experiments with a primary H_2 neutral molecule [30]. It is accepted that the higher the value of n the greater the degree of alignment of the molecular axis with respect to the laser polarization direction, and this has been shown to correspond to a reorientation of the molecular axis in the intense laser field. In the present case, the value of $n = 2$ suggests that no reorientation of the H_2^+, D_2^+ and HD^+ molecular ions occurs during dissociation, the $\cos^2\phi$ distribution merely mirroring the fall in $|E|^2$ (where E is the laser electric field vector) in the direction of the detector. This lack of alignment of the molecular ion indicates dissociation $(0,1)$ occurs at a very early stage on the rising edge of the laser pulse through the one photon process, allowing insufficient time for reorientation with the E vector to take place. Such dynamics would also explain the weakness of the two photon

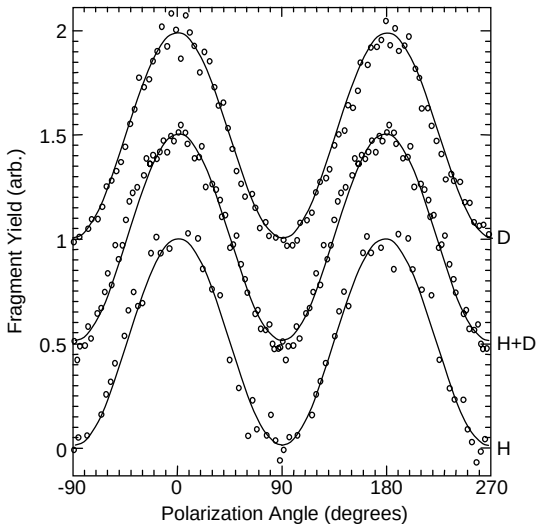

Fig. 8. Angular dependence of neutral fragment yields for fragmentation of (from top) D from D_2^+, the sum of H and D from HD^+, and H from H_2^+. The solid lines are a $\cos^2\phi$ fit to the experimental data.

absorption peak which would require a tighter alignment of the dipole moment with the laser field polarization.

5 Conclusion

We have investigated the response of beams of atomic and molecular ions to intense laser pulses. It is clear that the ionization and dissociation dynamics of ionic targets as compared to neutral targets is different, indicating a strong dependence on the primary ionized electron, demonstrating the need for further experimental and theoretical studies on positive ion targets. In the case of argon, we have shown that the removal of an electron prior to the arrival of the laser pulse almost completely suppresses nonsequential ionization. With a beam of C^+ as the target, a z-scan technique has demonstrated the separation of ground state and metastable components during ionization. Furthermore, ADK theory is demonstrated to hold only when the Keldysh parameter $\gamma < 1$. For molecular ions, different kinetic energy distributions were observed as compared to a neutral gas target. Furthermore, unlike the neutral case, no laser-induced reorientation was observed. Both of these observations indicate that the neutral molecule plays a formative role in the ionization dynamics of the H_2 molecule.

This work was supported by the Engineering and Physical Sciences Research Council (EPSRC).

References

1. K. Yamakawa, C.P.J. Barty, IEEE J. Sel. Top. Quant. Elec. **6**, 658 (2001)
2. A. L'Huiller *et al.*, in *Atoms in Intense Laser Fields*, edited by M. Gravrilla (Academic, New York, 1992), p. 139
3. M. Protopapas, C.H. Keitel, P.L. Knight, Rep. Prog. Phys. **60**, 389 (1997)
4. L.F. DiMauro, P. Agostini, Adv. At. Mol. Opt. Phys. **35**, 79 (1995)
5. C.J. Joachain, M. Dorr, N. Kylstra, Adv. At. Mol. Opt. Phys. **42**, 225 (2000); P. Lambropoulos, P. Margagakis, J. Zhang, Phys. Rep. **305**, 203 (1998)
6. A. Becker, F.H.M. Faisal, J. Phys. B: At. Mol. Opt. Phys. **32**, L335 (1999)
7. D. Dundas *et al.*, J. Phys. B: At. Mol. Opt. Phys. **32**, L231 (1999)
8. M.V. Ammosov, N.B. Delone, V.P. Krainov, Zh. Eksp. Teor. Fiz. **91**, 2008 (1986)
9. A.D. Bandrauk, M.L. Sink, J. Chem. Phys. **74**, 1110 (1981); A. Zavriyev *et al.*, Phys. Rev. A **42**, 5500-13 (1990)
10. L.J. Frasinski *et al.*, Phys. Rev. Lett. **83**, 3625 (1999)
11. A. Giusti-Suzor *et al.*, J. Phys. B: At. Mol. Opt. Phys. **28**, 309 (1995)
12. M. Schmidt *et al.*, Phys. Rev. A **50**, 5037 (1994)
13. J.H. Posthumus *et al.*, J. Phys. B: At. Mol. Opt. Phys. **28**, L349 (1995); T. Seideman *et al.*, Phys. Rev. Lett. **75**, 2819 (1995)
14. A.D. Bandrauk, in *21st Int. Conf. on the Physics of Electronic and Atomic Collisions*, Sendai, July 1999, edited by Y. Itikawa *et al.* (AIP Conf. Proc. 500, New York AIP, 2000), pp. 3-22
15. M. Brewczyk, K. Rzazewski, Phys. Rev. A **61**, 023412 (2000)
16. D. Stickland, G. Mourou, Opt. Commun. **55**, 447 (1985)
17. I.D. Williams *et al.*, Phys. Scripta T **80**, 534 (1999)
18. I.D. Williams *et al.*, J. Phys. B: At. Mol. Opt. Phys. **33**, 2743 (2000)
19. M.Y. Kuchiev, JETP Lett. **45**, 404 (1987)
20. P.B. Corkum, Phys. Rev. Lett. **71**, 1994 (1993)
21. H. van der Hart, K. Burnett, Phys. Rev. A **62**, 013407 (2000)
22. H.D. Hagstrum, Phys. Rev. **104**, 309 (1956)
23. P. Hansch, M.A. Walker, L.D. van Woerkom, Phys. Rev. A **54**, 4 (1996)
24. L. Zhang, L.J. Frasinski, K. Codling, J. Phys. B **27**, 3427 (1994)
25. L.V. Keldysh, Sov. Phys. JEPT **20**, 1307 (1965)
26. J.B. Greenwood *et al.*, Phys. Rev. A **88**, 233001 (2002)
27. I.D. Williams, J.B. Greenwood, B. Srigengan, R.W. O'Neill, I.G. Hughes, Meas. Sci. Technol. **9**, 930 (1998)
28. D. Pavičić, A. Kiess, T.W. Hänsch, H. Figger, Eur. Phys. J. D, e-print DOI: 10.1140/epjd/e2003-00197-2
29. K. Sändig, H. Figger, T.W. Hansch, Phys. Rev. Lett. **85**, 4876 (2000)
30. M.R. Thompson *et al.*, J. Phys. B: At. Mol. Opt. Phys. **30**, 5755 (1997)